Available online at www.sciencedirect.com
ScienceDirect
International Journal of Heat and Fluid Flow 29 (2008) 916–926
International Journal of HEAT AND FLUID FLOW
www.elsevier.com/locate/ijhff

Heat transfer with dimple/protrusion arrays in a rectangular duct with a low Reynolds number range

Sang Dong Hwang [a], Hyun Goo Kwon [b], Hyung Hee Cho [b,*]

[a] Korean Intellectual Property Office, Daejeon 302-701, Republic of Korea
[b] Department of Mechanical Engineering, Yonsei University, Seoul 120-749, Republic of Korea

Received 26 May 2007; received in revised form 8 November 2007; accepted 8 January 2008
Available online 5 March 2008

Abstract

This study investigated heat transfer characteristics on various dimple/protrusion patterned walls along with a straight and rectangular test channel. The dimple/protrusion arrays were positioned on one side of the wall (single) or on two sides of the wall (double) in each test case. The test duct was 15 mm in height and 105 mm wide. The print diameter of the dimple/protrusion was 12.99 mm and the height of the dimple/protrusion was 3.75 mm. Local heat transfer coefficients on the dimple/protrusion wall were measured using a transient TLC technique. Friction factors and performance levels are presented with the test cases. The Reynolds number, based on the duct hydraulic diameter, was varied from 1000 to 10,000.

From the results, thermal characteristics and performance levels were different in each test case. For the dimple wall case, on both the single and double-walls, thermal characteristics had similar patterns. However, flow mixing was higher for the double-wall than the single-wall, which resulted in enhanced heat transfer. As the Reynolds number decreased, the relatively low heat transfer region induced inside the dimple became wider and the local minimum of the heat transfer coefficient within the dimple moved downstream. For the protrusion wall case with the double-wall, the heat transfer coefficient increased greatly due to flow acceleration and stronger mixing flow. However, the heat transfer pattern was similar in both the single and double-wall cases. At high Reynolds numbers, the heat transfer pattern on the protrusion surface was 'pea-shaped' and upon decreasing the Reynolds number, the pattern became circular. Heat transfer enhancement was very high at low Reynolds numbers at both the dimple and protrusion walls. At $Re_{Dh} = 1000$, the enhancement levels were 14 and 7 for the double protrusion wall and the double dimple wall, respectively. However, at a high Reynolds number of 10,000, the enhancement level observed was from 2 to 3. For such a high heat transfer increment at the low Reynolds number, the performance factor is very high in this flow range. At a Reynolds number of 1000, the performance factors were 6.5 and 6 for the double protrusion wall and the double dimple wall, respectively.

Keywords: Heat transfer; Dimple; Protrusion; Low Reynolds number; Transient TLC

1. Introduction

Heat transfer enhancement in a duct/channel is of great interest and importance in many industrial applications such as gas turbines, heat exchangers, and various cooling devices because higher heat transfer rates increase system efficiency and reduce thermal load. For these reasons, many studies have been conducted on various enhancement techniques in an internal passage to increase the heat transfer rates of target systems. For heat transfer enhancement, various techniques such as rib turbulators, pin arrays, arrays of shaped roughness elements, and dimples have been used in practical systems. Among these enhancement techniques, interest in dimples has recently increased due to the relatively low pressure penalty compared to other enhancement techniques.

Chyu et al. (1999) reported local heat transfer measurements on two different concave shape (hemispheric and

* Corresponding author. Tel.: +82 2 2123 2828; fax: +82 2 312 2159.
E-mail address: hhcho@yonsei.ac.kr (H.H. Cho).

0142-727X/$ - see front matter © 2008 Elsevier Inc. All rights reserved.
doi:10.1016/j.ijheatfluidflow.2008.01.004

Nomenclature

AR	aspect ratio (W/H)
D	dimple diameter
D_h	duct hydraulic diameter
d	dimple print diameter
f	friction factor in Eq. (5)
f_0	friction factor for smooth duct
H	duct height
H_d	dimple depth
H_p	protrusion height
h	convective heat transfer coefficient
k	thermal conductivity
L	duct length
Nu	Nusselt number in Eq. (3)
$\underline{Nu}_0$	Nusselt number for smooth duct
$\overline{Nu}$	averaged Nusselt number in Eq. (4)
P	dimple or protrusion pitch (Fig. 2)
ΔP	pressure drop per unit length
PF	performance factor in Eq. (6)
Re_{Dh}	Reynolds number based on hydraulic diameter
t	time of color change
T	temperature
U	average duct inlet velocity
W	duct width
x	stream-wise coordinate (Fig. 2)
y	distance from the wall (Fig. 2)
z	span-wise coordinate (Fig. 2)

Subscripts

d	dimple wall
i	initial condition
p	protrusion wall
r	reference condition
w	wall condition

Greek symbols

α	thermal diffusivity
ρ_{air}	density of air

teardrop) using a transient liquid crystal technique. They obtained about a 2.5 times greater heat transfer enhancement and a relatively low pressure penalty. Moon et al. (2000) investigated effects of the channel height on heat transfer in a rectangular duct with a dimpled surface and found that the dimple indentations enhanced the heat transfer level by about 2.1 times, regardless of the channel height. Mahmood and Ligrani (2002) measured local heat transfer on the dimpled surface with various temperature ratios at a Reynolds number of 10,000. Moon and Lau, 2002 showed that concave and cylindrical dimple configurations enhanced the overall heat transfer rates by 1.7 times. Burgess et al. (2003) conducted an experimental study to investigate the effects of dimple depth on heat transfer enhancement. As a result, they showed that the local and spatially-resolved Nusselt number augmentations increased with the dimple depth. Ligrani et al. (2001) presented flow characteristics for the channel with the dimple wall having protrusions on the opposite walls using flow visualization and reported the local heat transport distributions. They found that the heat transfer coefficients were enhanced by the protrusions on the top wall and these protrusions caused more mixing and vortices which increased the overall Nusselt number and as well as pressure drop.

It is well known that at high Reynolds numbers (above 10,000), the heat transfer enhancement level by the dimples maintains nearly constant of 2.3–2.5 regardless of the Reynolds number. There is, however, insufficient data at low Reynolds number conditions. Particularly, in compact heat exchanger applications, flow conditions are mostly at low Reynolds numbers. Therefore, heat transfer and pressure drop characteristics in the laminar/transition flow regimes in a rectangular duct are needed. Wang et al. (2003) revealed the existence of a 3D 'horse-shoe' vortex inside single dimples in a laminar channel. But not much local heat transfer and pressure drop data exist regarding the laminar/transient flow channel with a dimpled wall.

In this study, therefore, local heat transfer characteristics in a rectangular duct with dimple or a protrusion arrays were investigated at low Reynolds numbers ($Re_{Dh} =$ 1000–10,000). To characterize the effects of the roughened surfaces containing dimples and protrusions on heat transfer rates, four different roughened surfaces (single dimple wall, double dimple wall, single protrusion wall, and double protrusion wall) were studied. Also, the augmentation levels for these different surface conditions were evaluated by comparing the heat transfer increments with pressure loss.

2. Experimental apparatus and procedures

2.1. Experimental setup

Fig. 1 shows a schematic diagram of the experimental setup for the heat transfer experiments for the dimple/protrusion surfaces using a transient Thermochromic-Liquid-Crystal (TLC) technique. This setup consists of a blower, heat exchanger, orifice meter, air-heater, solenoid valves, plenum and test section. The blower (5 HP) supplies the main flow and the flow rates are controlled by an inverter (Samsung, Moscon G5). The main flow passes through the heat exchanger to maintain constant temperature. Flow rates are measured by the orifice meter, which was designed according to ASME (ASME Research Committee on Fluid Meters, 1961) and Bean (Bean, 1974). A pipe type air-heater (2 in. I.D., 3.5 kW, Hyundai Heaters) was installed between the orifice meter and the bypass valve to heat

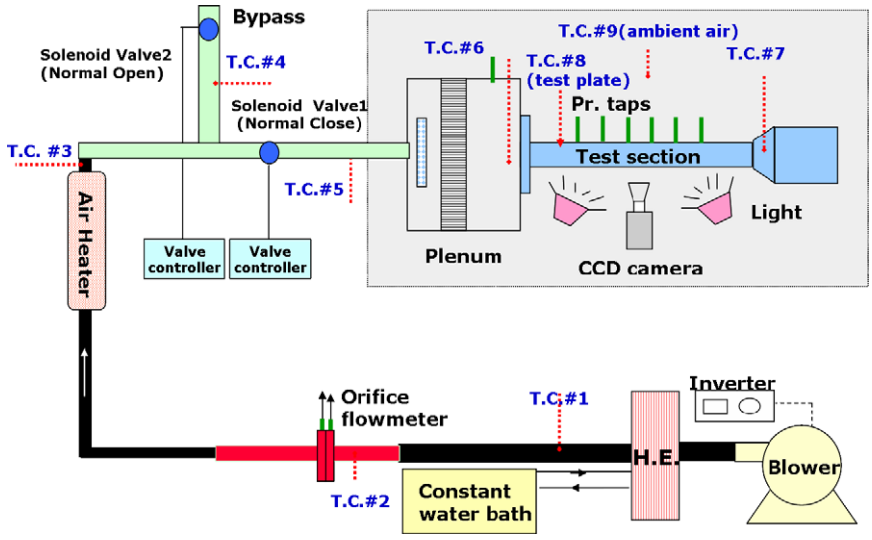

Fig. 1. Schematic diagram of overall experimental setup.

the main flow. Two different types of solenoid valves are installed before the test section to control flow direction. The solenoid valve #1 (Korcon, VPW229-N-A22) is the normal open type and the solenoid valve #2 (Korcon, VDW216-N-A22) is the normal close type.

To capture TLC images in the test sections, a color CCD camera (CV-m77, JAI) which has 1024 by 768 resolutions with a fixed focal length lens (C1614A, 16 mm, F1.4, Cosmicar) and frame grabber (Corona-II, Matrox) was used. Also, four compact type florescent lamps (Ex-D, Kumho Electric Inc.) with a 6500 K color temperature with an electric ballast stabilizer were used as the lighting system. A total of nine thermocouples (J type, 36 gauge, Omega) were installed to monitor flow temperatures.

The rectangular duct used in this study had various wall patterns in each case. Schematic diagrams of the test surfaces are shown in Fig. 2. The height of the duct (H) was 15 mm and the width (W) was 105 mm. The aspect ratio (W/H) of the test duct was 7 and the duct hydraulic diameter (D_h) was 26.25 mm. The upstream developing length was 265 mm (over 10 D_h) and the length (L) of the test plate was 190 mm. The test plate contained 12 rows of dimples or protrusions.

The dimple diameter (D) was 15 mm and the dimple depth (H_d) was 3.75 mm (0.25 D) while the print diameter of the dimples (d) was 12.99 mm. The protrusion diameter and height (H_p) were the same as those used in the dimple case. The duct height normalized by dimple depth or protru-

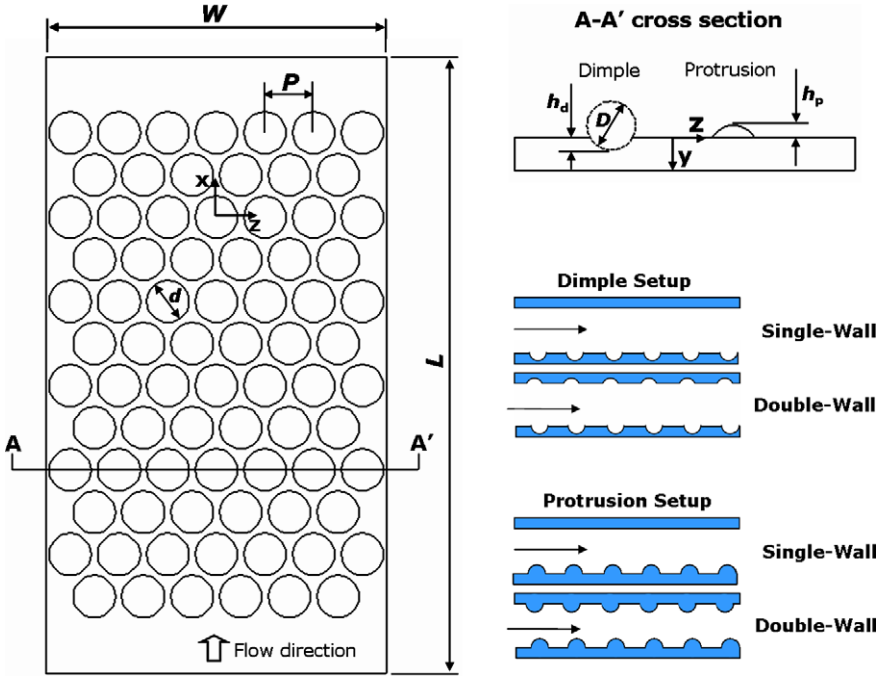

Fig. 2. Test section arrangement.

sion height (H/H_d or H/H_p) was 4. The test plate was 10-mm thick transparent acryl. For the transient TLC technique, a sprayable TLC containing R30C5W (SPNR30 C5W, Hallcrest Inc.) and black paint (SPBB, Hallcrest Inc.) was used because of the complex shapes of the test plate.

Fourteen pressure taps with a 1.0 mm diameter were drilled at the duct side to measure the pressure drop. The pressure taps were positioned 25.0 mm interval in the test section. The pressure drops were measured using a digital micromanometer (DPI-145, Druck) with an indicator (LPE-9145, Druck).

The Reynolds numbers used in this study, based on the duct hydraulic diameter (Re_{Dh}), ranged from 1000 to 10,000 (1000, 3000, 5000 and 10,000).

2.2. Transient TLC technique

A transient TLC technique was applied to acquire the heat transfer coefficient distributions on the dimpled/protruded surface. In the transient heat transfer experiment, the heat transfer coefficient (h) was calculated from the one-dimensional transient conduction equation over a semi-infinite solid. In addition, a step rise of temperature is used in this method. The well known solution is represented by the following Eq. (1) (Arpaci, 1966).

$$\frac{T_w - T_0}{T_r - T_0} = 1 - \exp\left(\frac{h^2\alpha t}{k^2}\right)\mathrm{erfc}\left(\frac{h\sqrt{\alpha t}}{k}\right) \tag{1}$$

Hence, the heat transfer coefficient can be calculated from the above Eq. (1) once the initial temperature (T_i), mainstream reference temperature (T_r), wall temperature (T_w) and time of color change (t) are known. In practice, however, it is impossible to provide a step temperature rise in fluid temperature. So, by applying Duhamel's superposition principle to the above solution (Rohsenow et al., 1997 and Arpaci, 1966), Eq. (1) becomes:

$$T_w - T_i = \sum_{j=1}^{N}\left[1 - \exp\left(\frac{h^2\alpha(t-t_j)}{k^2}\right)\mathrm{erfc}\left(\frac{h\sqrt{\alpha(t-t_j)}}{k}\right)\right] \times (T_{r,j} - T_{r,j-1}). \tag{2}$$

Another important consideration is the thickness of the test plate and run time. The assumption of a semi-infinite solid is valid as long as the material is of sufficient thickness to prevent heat from penetrating through the wall within the test run time. Hence, the thickness of the test plate and the test time were determined from a correlation, $y = 2(\alpha t)^{0.5}$ (Schultz and Jones, 1973), to satisfy the assumption of the one-dimensional condition.

2.3. Data reduction

The dimensionless heat transfer coefficient, the Nusselt number, is defined as:

$$Nu = \frac{hD_h}{k} \tag{3}$$

The test section has 12 rows of dimple/protrusion array in staggered arrangement. We present the average heat transfer coefficients at the 8th row for the stream-wise direction and central dimple/protrusion region for the span-wise direction, which is $1.0 \leqslant x/d \leqslant 1.0$ and $-0.5 \leqslant z/d \leqslant 0.5$.

The averaged Nusselt number is obtained by following numerical integration

$$\overline{\overline{Nu}} = \frac{\int_{x/d=-1}^{x/d=1}\int_{z/d=-0.5}^{z/d=0.5} Nu\,dz\,dx}{A} \tag{4}$$

The friction factor, f, is defined as:

$$f = \frac{\Delta P}{4(1/D_h)(1/2)\rho_{air}U^2} = \frac{1}{2}\Delta P\frac{D_h}{\rho_{air}U^2} \tag{5}$$

where ΔP, ρ_{air}, and U are the pressure drop along the test section, the density of air, and the average velocity at the duct inlet, respectively. The friction factor is obtained by linearly fitting the slope of pressure drop at the test section including the entrance region.

The performance factor, PF, is obtained by considering both heat transfer enhancement and the pressure loss increment based on a constant pumping power condition. The performance factor is defined as: (Gee and Webb, 1980)

$$\mathrm{PF} = \frac{Nu/Nu_0}{(f/f_0)^{1/3}} \tag{6}$$

where Nu_0 and f_0 are the Nusselt number and friction factor of the smooth wall case, respectively. The Nusselt number and friction factor for the smooth wall case were also measured using the same experimental setup and conditions.

2.4. Uncertainty estimate

An uncertainty analysis of the Nusselt number and the friction factor has been conducted based on the analysis of Abernethy et al. (1985) with a confidence level of 95%. The Nusselt number uncertainty was 8% for the entire operating range of the experiments. This uncertainty is attributed mainly to the properties of the test plate and the wall temperature measured by the TLC (about 5%). Also, the uncertainty of friction factor was about 4.4%.

3. Results and discussion

3.1. Local heat transfer characteristic

In a channel roughened with dimples or protrusions, various flow vortices appear. These vortices augment heat transfer coefficients on the surfaces. There are characteristic flow patterns in each case of the dimple wall and the protrusion wall. For the dimple wall cases, three induced flow types mainly enhance heat transfer; separation/reattachment flow, downward/upwash flow, and vortex sheddings. These vortices affect heat transfer characteristics

on the dimple surface. In case of double dimple wall, also, the upwash flow induced by the one wall interacts with the vortices generated from the opposite wall. These interactions enhance the heat transfer coefficients on the rear part of inside of dimple and on the downward flow region of the dimple. For the protrusion wall cases, also, three induced flow characteristics appear; main flow impingement and vortex legs at both sides of the protrusion, and flow separation.

Fig. 3 shows contours of the Nusselt number for dimple walls with decreasing Reynolds number. The dimples are arranged in a staggered array pattern. The single-wall represents the case when the dimples were installed only on the side of the rectangular duct (top wall), and the double-wall indicates the case where the dimples were installed on two sides of the rectangular duct (both top and bottom walls). The dashed circle in Fig. 3 represents the dimple edges. The dimple pattern on the top and bottom walls for the double-wall case was aligned without an offset. The main flow direction is from the left to right side.

For the single-wall dimple case at a relatively high Re ($Re_{Dh} = 10{,}000$), high heat transfer regions appeared at the rear and diagonal rims of the dimpled surface due to the upwash flow at the rear rim of the dimple edge, the phenomenon that is well-known. In addition, a pair of vortices appeared at the diagonal side. These vortices originating inside a dimple were visualized and interpreted by Mahmood and Ligrani (2002). Inside the dimple, a low heat

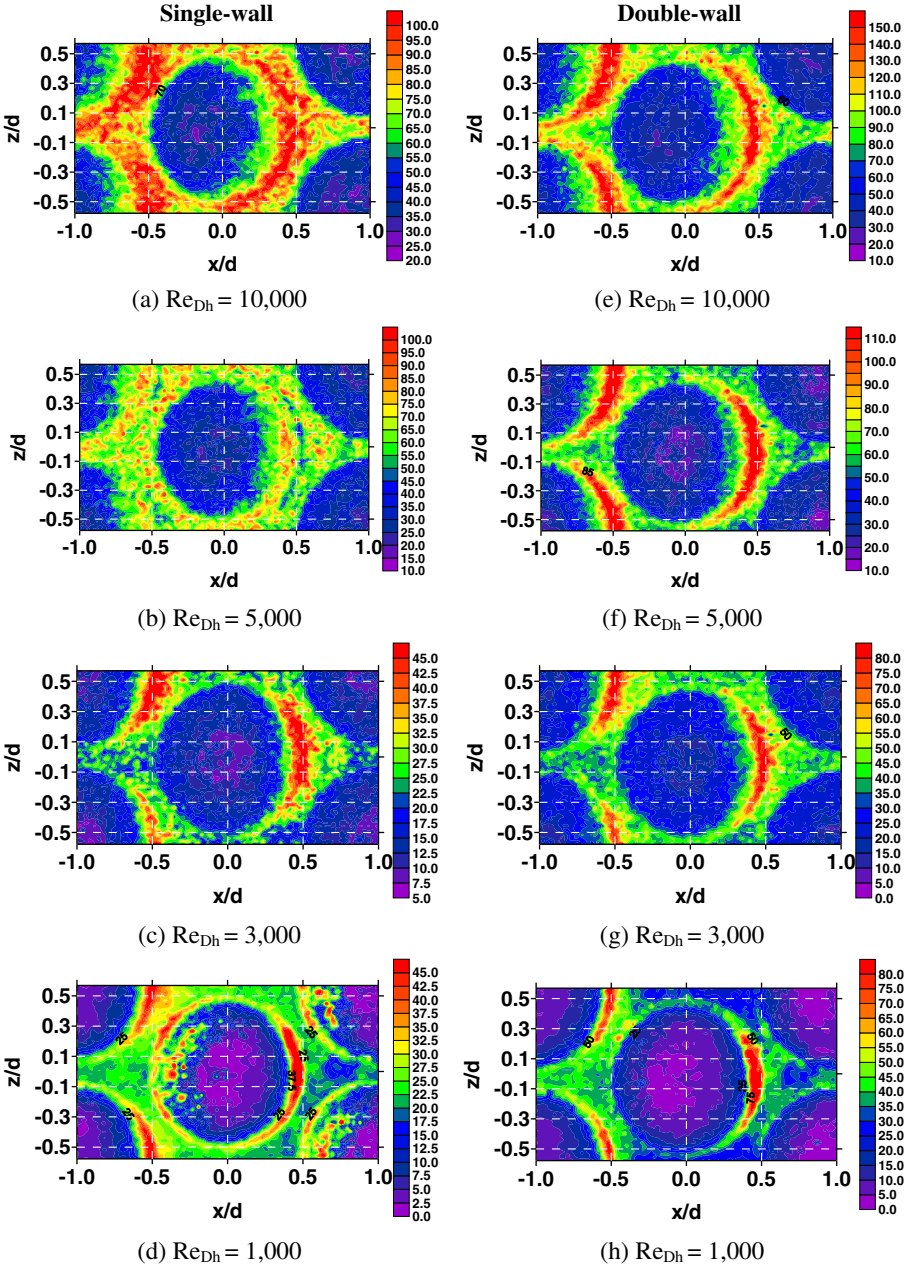

Fig. 3. Contours of Nusselt number for dimple walls with decreasing Reynolds number.

transfer region appears due to flow separation and recirculation. The detailed flow and heat transfer characteristics for the dimpled case at $Re_{Dh} = 10{,}000$ are also detailed in our previous study (Hwang and Cho, 2005).

When the Reynolds number decreased, overall heat transfer patterns were similar to those for the Reynolds number of 10,000, i.e. the low heat transfer region appeared inside the dimple and the high heat transfer region appeared at the rear side of dimple. However, as the Reynolds number decreased, two definite features were discovered. One is that the low heat transfer region inside the dimple becomes wider and the other is that the local minimum of the heat transfer coefficient inside the dimple moved toward the physical center of the dimple. This is because the size of the recirculation zone becomes larger due to decreased flow velocity. These heat transfer characteristics appeared in the same manner as the Reynolds number decreased for both the single and double dimple walls. However, the heat transport level for the double dimple wall case was higher than that for the single dimple wall case due to enhanced flow mixing.

The stream-wise and span-wise local Nusselt number distributions on the dimple walls are shown in Fig. 4. The dashed lines indicate the dimple edges. Regardless of the Reynolds number, the overall heat transfer patterns are similar to each other. The local peak of the heat transfer coefficient by the upwash flow and shedding vortices appears at a position of $x/d = 0.5$ and $z/d = 0.0$. Within the dimple, a relatively low heat transfer rate exists by flow recirculation. As mentioned above, as the Reynolds number decreased, the low heat transfer regions became wider in the span-wise direction and the local valley of heat transfer coefficients moved towards downstream. The Nusselt number distributions for the double dimple wall have a similar pattern to those for the single dimple wall. However, for the double-wall case, enlarged vortex strength by the vortices generated by opposite side affects the duct walls, which result in heat transfer enhancements. This enhancement by the opposite wall is dominantly marked on the flat surface without dimples. Inside the dimple region, there is little difference in heat transfer enhancement among the single and double dimple wall cases.

The Nusselt number distributions for the protrusion wall case are shown in Fig. 5. The dashed circles represent the protrusion edges. For the protrusion surface, the main flow impinges on the front side of protrusion, and 'horse-shoe' vortices are generated by the existence of an obstacle. A low heat transfer region appears at the rear side of the protrusion due to wake flow. In addition, a pair of vortex legs originated at the former protrusion affects the downstream protrusions located in the diagonal direction. These vortex legs augment the heat transfer coefficients on the rear

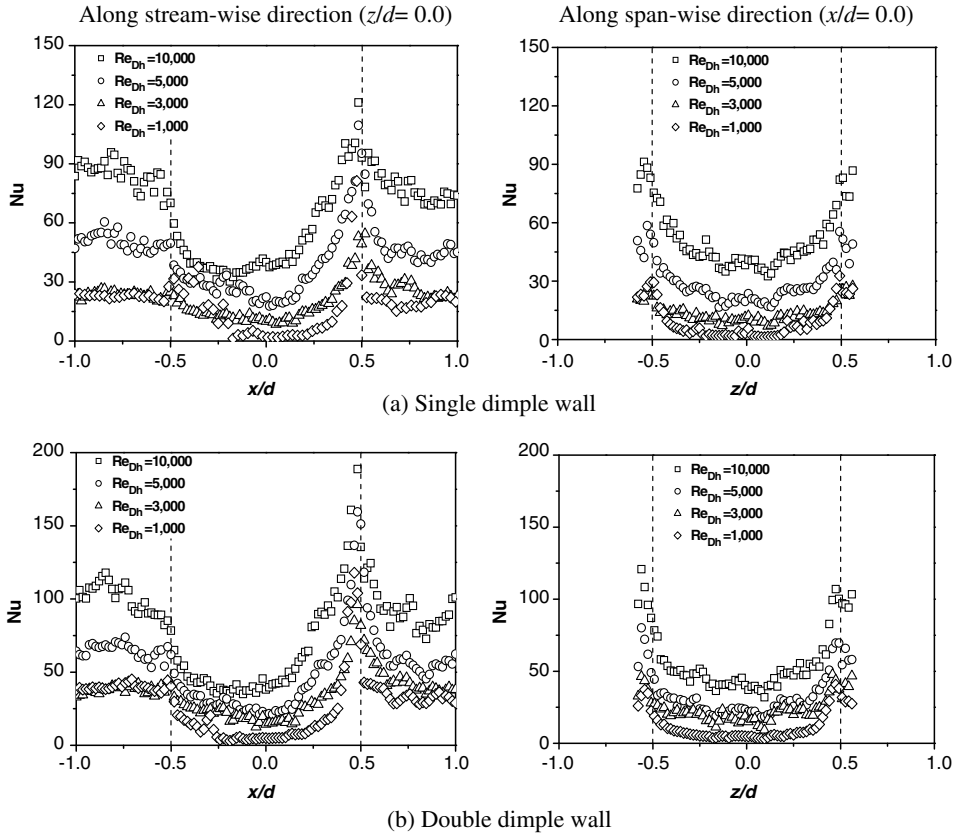

Fig. 4. Local Nusselt numbers for dimple walls with decreasing Reynolds number along stream-wise direction ($z/d = 0.0$) and span-wise direction ($x/d = 0.0$). (a) Single dimple wall; (b) double dimple wall.

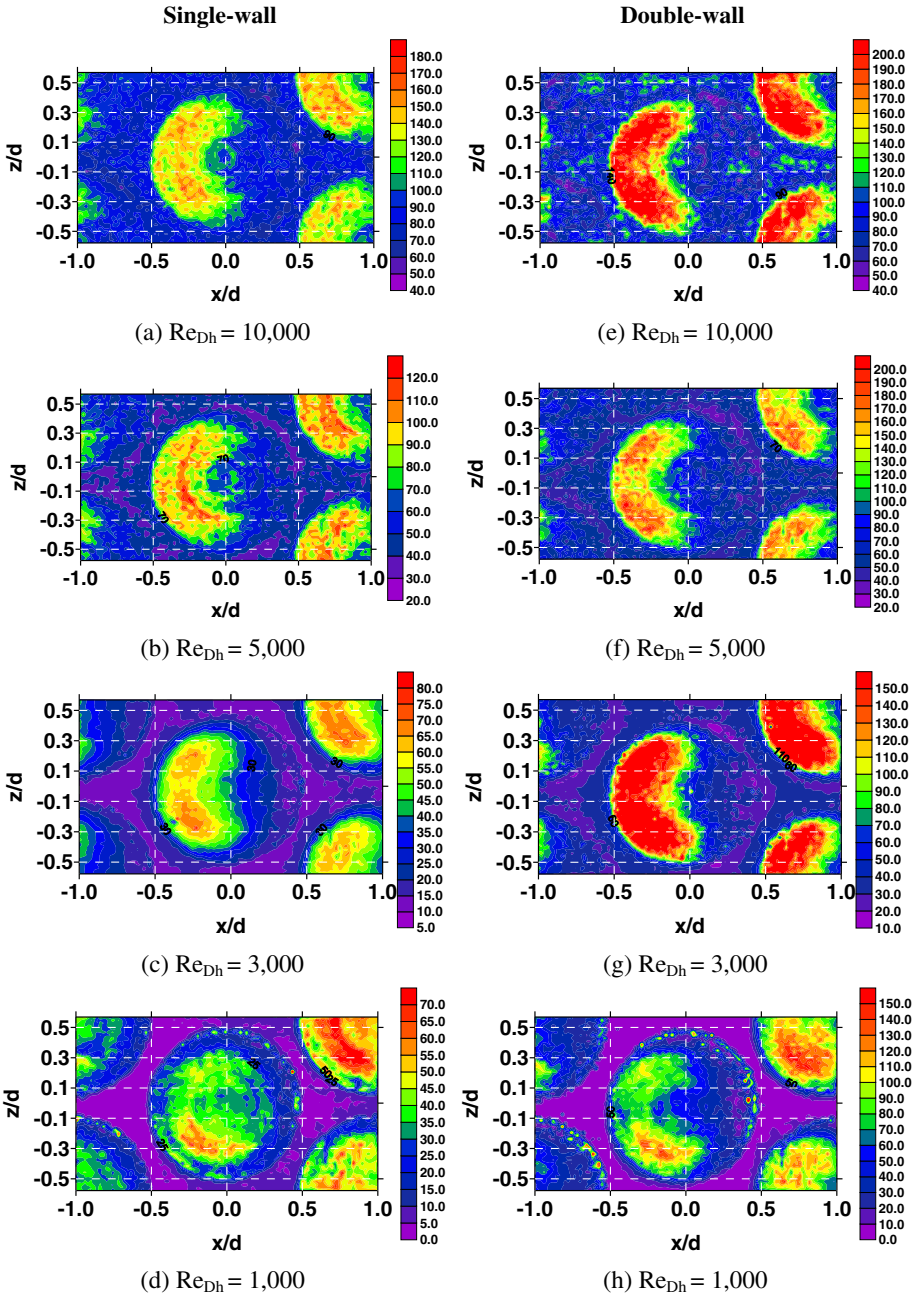

Fig. 5. Contours of Nusselt number for protrusion walls with decreasing Reynolds number.

diagonal protrusions. Hence, a 'pea-shaped' high heat transfer region appears on the protrusion surface. However, with decreasing Reynolds number, the 'pea-shape' contours of heat transfer coefficients on the front side of protrusion surface become circular shape at the low Reynolds number for the single protrusion wall case. For the double protrusion wall case, heat transfer characteristics appear in a similar manner to those for the single-wall. However, the local Nusselt number for the double protrusion wall is higher than that for the single-wall due to the flow acceleration and the vortices induced on the opposition wall.

Local Nusselt number distributions along the stream-wise and span-wise directions for the protrusion wall are shown in Fig. 6. In the single protrusion wall case (Fig. 6a), high heat transfer coefficients appear at the front side of the protrusion at about $x/d = -0.4$ along the stream-wise direction and $z/d = \pm 0.3$ along the span-wise direction due to the impinging effects of the main flow and vortices induced by the former protrusions, as explained above. For the span-wise distribution, two local peaks in the heat transfer coefficients exist due to the 'horse-shoe' vortex legs caused by former protrusions. As the Reynolds number decreases, the heat transfer coefficients become lower. Heat transfer characteristics for the double protrusion wall case (Fig. 6b) show patterns qualitatively similar to those in the single-wall case. The local

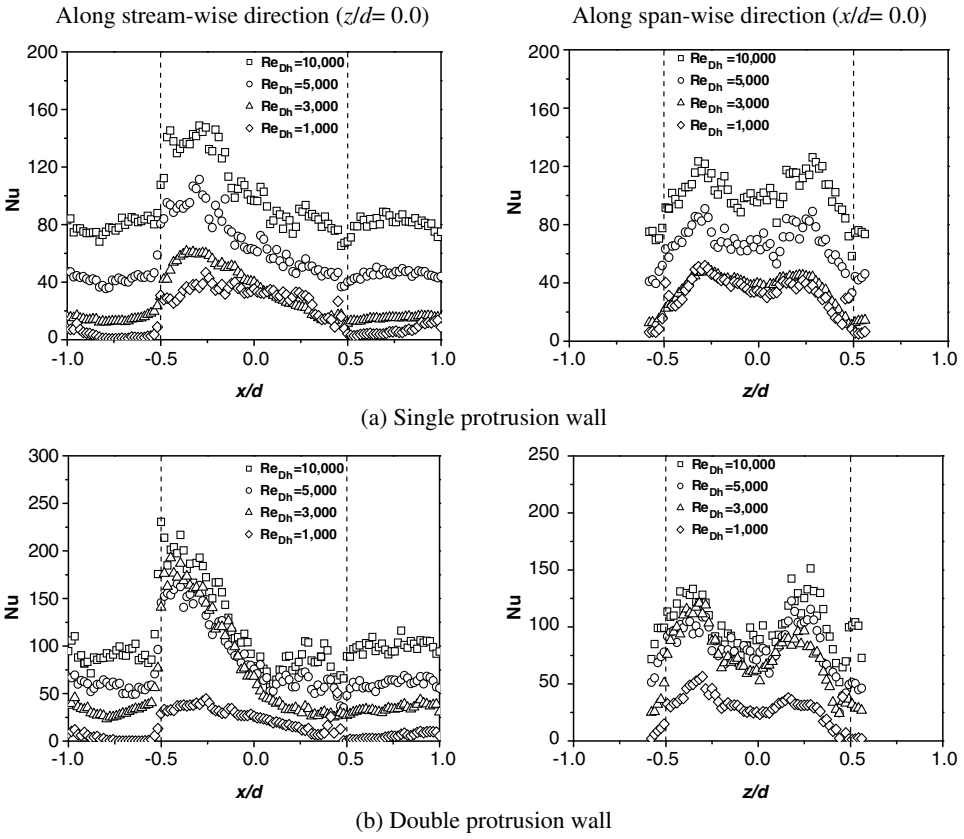

Fig. 6. Local Nusselt numbers for protrusion walls with decreasing Reynolds number along stream-wise direction ($z/d = 0.0$) and span-wise direction ($x/d = 0.0$). (a) Single protrusion wall; (b) double protrusion wall.

peaks of heat transfer due to impingement of the main flow and by the vortex legs appear at the same positions as those for the single protrusion wall case. For the Reynolds numbers from 3000 to 10,000, all the test cases show similar Nusselt number distributions. However, at the lowest Reynolds number of 1000, the Nusselt numbers are very low, similar to those for the single case. It is presumed that the different flow and thermal characteristics are induced by the vortex interactions generated at the opposite protrusions.

3.2. Averaged heat transfer distributions

Fig. 7 shows the average Nusselt numbers for various Reynolds numbers. The averaged Nusselt number distributions with the Reynolds numbers are presented in Fig. 7a. The solid line represents the predicted Nusselt number in laminar flow by Shah and London (1978) for the case of uniform temperature at the four walls. The dotted line shows Dittus and Boelter's correlation (Dittus and Boelter, 1985) for fully developed turbulent flow in a smooth circular duct. In the case of the smooth rectangular duct with an aspect ratio of 7, the Nusselt numbers are in good agreement with the predictions.

For the dimple wall case, the average heat transfer rates of the double-wall are higher than those of the single-wall with the increased flow mixing due to interaction between vortices generated from both upper and lower walls. However, higher vortex interactions in the duct with both dimpled walls appear mainly at the low Reynolds number below 3000. As shown in Fig. 7b, at the Reynolds number of 1000, heat transfer enhancement of double-wall is 7.0 and single-wall is 5.4. For the relatively high Reynolds number range, the vortex interaction becomes weaker due to higher momentum of the main flow. Thus the normalized average Nusselt number for the dimple wall decreases with increasing the Reynolds number about $Re_{Dh} = 5000$. At the high Reynolds number over 5000, the dimensionless average heat transfer rates maintain a nearly constant value of 2.0. Hence, the effect of the wall pattern on heat transfer augmentation is significant in the low Reynolds number region, such as laminar/transition flow regime.

For the protrusion wall case, the overall Nusselt number is relatively higher than that of the dimple wall case. In the case of the single protrusion wall, the average Nusselt number coincides with that of the double dimple wall case because of higher secondary flows (Fig. 7a). The average Nusselt number increases greatly for the double protrusion wall case. This is due to the acceleration of main flow with reduced flow cross-sectional area and the interaction between vortices generated by the opposite side wall. In the low Reynolds number range, the normalized average Nusselt number for the double protrusion wall is much higher than that in the smooth duct flow. In particular,

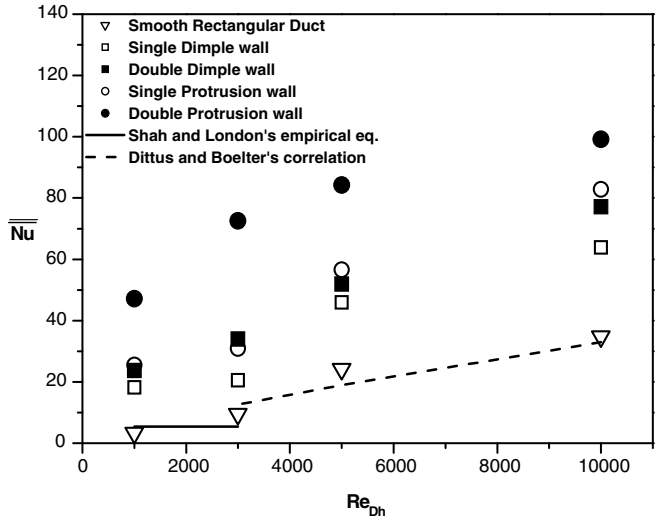

(a) Average Nusselt number

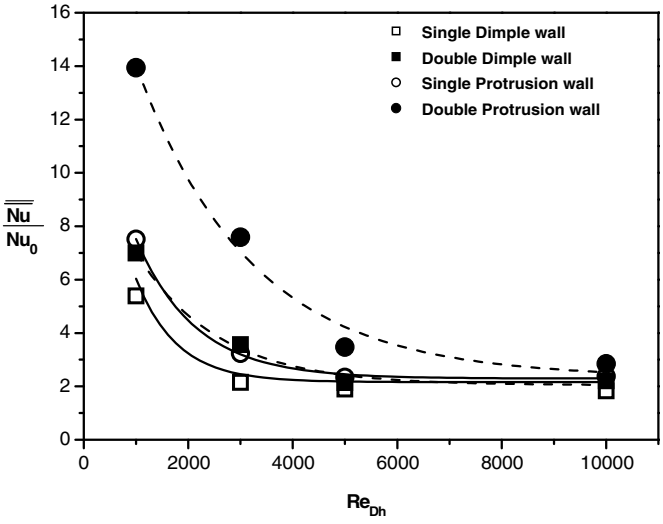

(b) Normalized average Nusselt number

Fig. 7. Average Nusselt numbers for various Reynolds numbers. (a) Average Nusselt number; (b) normalized average Nusselt number.

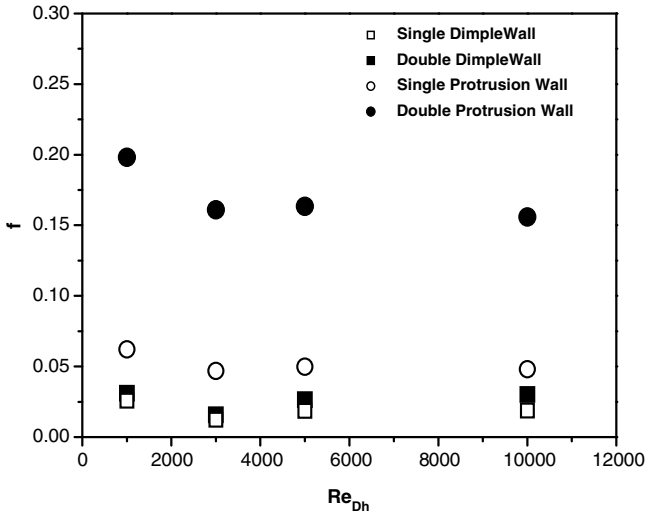

(a) Friction factor

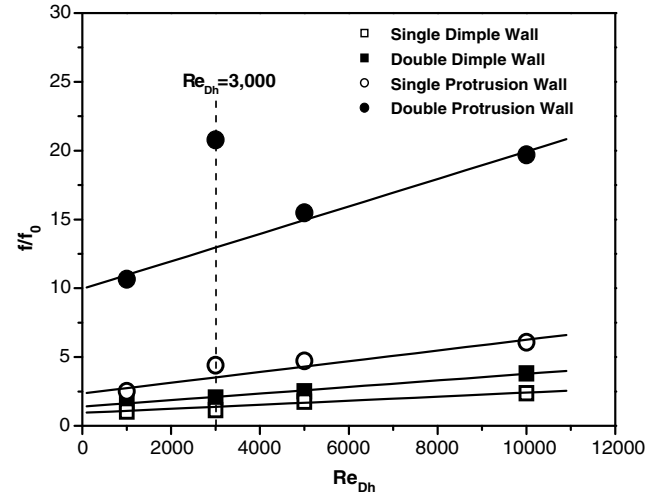

(b) Normalized friction factor

Fig. 8. Friction factors for various Reynolds numbers. (a) Friction factor; (b) normalized friction factor.

at the Reynolds number of 1000, the normalized average heat transfer coefficient increases up to 14. However, in the high Reynolds number range ($Re_{Dh} \geqslant 5000$), the heat transfer augmentation maintains a constant value of about 2.0–3.0.

3.3. Pressure drop and performance factor

Fig. 8 presents friction factors for the various Reynolds numbers. As can be seen in Fig. 8a, the friction factors of all the cases decrease with increasing the Reynolds number for $Re_{Dh} \leqslant 3000$, then maintain nearly constant values at the higher Reynolds numbers. For the normalized friction factors in Fig. 8b, both single and double dimple wall cases show the lowest normalized friction factor of about 2.5–3.0. That is, the dimple wall case shows a lower pressure drop increment compared to the protrusion wall cases due to enlargement of flow cross-sectional area. For the protrusion wall cases, however, relatively high friction factors are obtained. In particular, the double protrusion wall case shows the high value of 10–22 within the tested ranges. In particular, at $Re_{Dh} = 3000$, the normalized friction factor for the double protrusion wall case increases rapidly due to the acceleration of main flow with reduced flow cross-sectional area (blockage effect) and the strong interaction of induced secondary vortices.

In general, heat transfer enhancement is important in increasing heat transfer rates and enlarging surface areas. Pressure loss related to pumping power is also important because the pressure loss increases generally with the heat transfer rates increasing. Hence, the performance factor, which considers both heat transfer enhancement and pressure loss increment, is proposed to evaluate the augmentation levels. Fig. 9 presents the performance factors for the dimple and protrusion wall cases. For the dimple wall cases, the performance factor is very high at low Reynolds

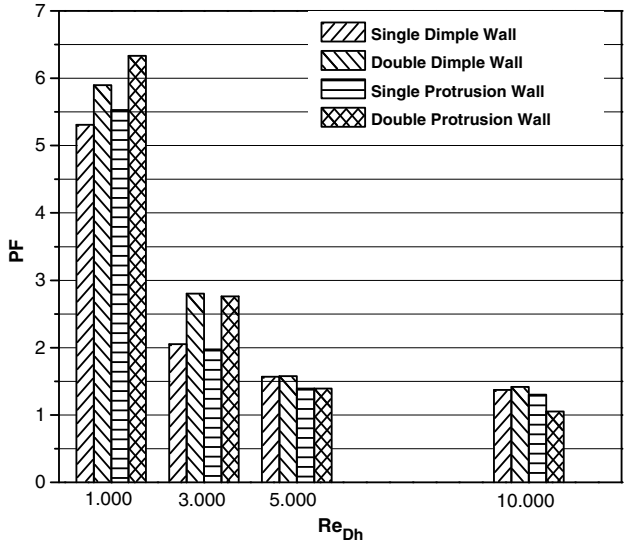

(a) Performance factors

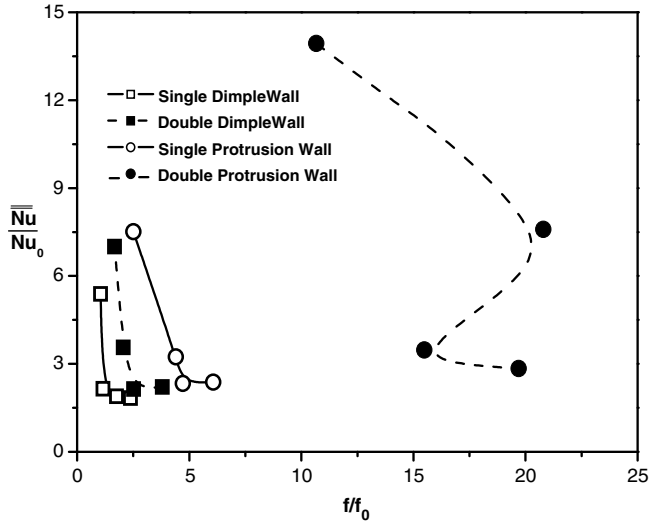

(b) Average Nusselt number ratio vs. friction factor ratio

Fig. 9. Performance factor distributions. (a) Performance factors; (b) average Nusselt number ratio vs. friction factor ratio.

number of 1000 and lower at the higher Reynolds numbers. The performance factor at $Re_{Dh} = 3000$ is about 2 (single) to 3 (double) and the performance factor at $Re_{Dh} = 1000$ is about 5 (single) to 6 (double). Therefore, the performance factor at the low Reynolds number of 1000 is about 2 (double) to 2.5 (single) times higher than that at the high Reynolds number. This is due to effects of the secondary flow vortices induced by the dimples which results in large heat transfer enhancement but relatively low pressure drop increases at the low Reynolds number for the dimple cases with enlargement of flow cross-sectional area. In addition, the double dimple wall case results in a higher value than that for the single dimple wall case due to the more heat transfer enhancement with the increased strength of the secondary flow vortices. The friction factors, however, for both single and double dimple walls are nearly identical in all Reynolds number of this study.

At the high Reynolds numbers, above 5000, the performance factors show no discrepancy between the single and double dimple wall cases because the pressure drop increase is higher than the heat transfer enhancement for the double dimple wall. For the protrusion wall cases, the double protrusion wall case shows the highest performance factor at the Reynolds number of 1000 and the performance factor is also higher than that of the single-wall case at the Reynolds numbers of 3000. However, at the high Reynolds numbers above 5000, the performance factors remain lower. In particular, at the highest Reynolds number of 10,000 in the present study, the double protrusion wall case shows the lowest value due to the greatly increased pressure drop. As a result, the double protrusion wall case shows the highest performance level at the low Reynolds number of 1000 due to its dramatic heat transfer enhancement. As the Reynolds number increases, the performance level becomes similar for the all test cases. At the high Reynolds number, the dimple case shows a slightly higher performance level than that of the protrusion wall case due to the lower pressure drop of the dimple wall case, even though the protrusion wall case shows higher heat transfer enhancement.

4. Conclusions

In the present study, the local heat transfer coefficients and friction factors were obtained for a rectangular duct with dimples or protrusions which were installed at the top wall only (single-wall) or both top and bottom walls (double-wall). These measurements were carried out mainly at low Reynolds numbers ($1000 \leqslant Re_{Dh} \leqslant 10{,}000$). The conclusions of the present study are summarized as follows:

(1) *Local heat transfer characteristics*
For the single dimple wall case, the low heat transfer region appears inside the dimple and the high heat transfer region appears at the rear side of dimple. As the Reynolds number decreases, the low heat transfer region becomes wider and the local minimum of heat transfer coefficients inside the dimple moves downstream. For the protrusion wall case, a 'pea-shaped' high heat transfer region appears at the front side of the protrusion and a low heat transfer region exists at the rear side of the protrusion. However, upon decreasing the Reynolds number, the 'pea-shaped' region becomes circular.

(2) *Average heat transfer*
The overall heat transfer coefficient is higher for the double-wall than the single wall. Particularly, for the double protrusion wall, the averaged heat transfer rate is the highest due to the flow acceleration and high flow mixing. The enhancement level of heat transfer is very high at the low Reynolds numbers. At the Reynolds number of 1000, the enhancement level is 14 and 7 for the double protrusion wall and

double dimple wall, respectively. However, at a high Reynolds number, the enhancement remains constant at a low level of about 2–3.

(3) *Pressure drop and performance factor*
The pressure drop in the double protrusion wall case is the highest due to the blockage effect. However, for the double dimple wall case, the pressure drop increment is similar to the single dimple wall case. The performance factor is high at the low Reynolds number due to the great increase of heat transfer. For $Re_{Dh} = 1000$, the PF is about 6.5 and 6.0 for the double protrusion wall and the double dimple wall, respectively.

References

Abernethy, R.B., Benedict, R.P., Dowdell, R.B., 1985. ASME measurement uncertainty. ASME Journal of Fluid Engineering 107, 161–164.

Arpaci, V.S., 1966. Conduction Heat Transfer. Addison-Wesley.

ASME Research Committee on Fluid Meters, 1961. Flow Meter Computation Handbook. ASME, NY.

Bean, H.S., 1974. Fluid Meters: Their Theory and Application, sixth ed. ASME, NY.

Burgess, N.K., Oliveira, M.M., Ligrani, P.M., 2003. Nusselt number behavior on deep dimpled surfaces within a channel. Journal of Heat Transfer 125, 11–18.

Chyu, M.K., Yu, Y., Ding, H., 1999. Heat transfer enhancement in rectangular channels with concavities. Enhanced Heat Transfer 6, 429–439.

Dittus, P.W., Boelter, L.M.K., 1985. Heat transfer in automobile radiators of the tubular type. International Communications in Heat Mass Transfer 12, 3–22.

Gee, D.L., Webb, R.L., 1980. Forced convection heat transfer in helically rib-roughened tubes. International Journal Heat Mass Transfer 23, 1127–1135.

Ligrani, P.M., Mahmood, G.I., Harrison, J.L., Clayton, C.M., Nelson, D.L., 2001. Flow structure and local Nusselt number variations in a channel with dimples and protrusions on opposite walls. International Journal of Heat and Mass Transfer 44, 4413–4425.

Mahmood, G.I., Ligrani, P.M., 2002. Heat transfer in a dimpled channel: combined influences of aspect ratio, temperature ratio, Reynolds number, and flow structure. International Journal of Heat and Mass Transfer 45, 2011–2020.

Moon, S.W., Lau, S.C., 2002. Turbulent heat transfer measurements on a wall with concave and cylindrical dimples in a square channel. ASME Paper GT-2002-30208.

Moon, H.K., O'Connell, T., Glezer, B., 2000. Channel height effect on heat transfer and friction in a dimpled passage. Journal of Engineering for Gas Turbines and Power 122, 307–313.

Rohsenow, W.M., Hartnett, J.P., Cho, Y.I., 1997. Handbook of Heat Transfer, third ed. McGrawHill, pp. 14.47–16.50.

Sang Dong Hwang, Hyung Hee Cho, 2005. Heat transfer of internal passage using dimple/protrusion. In: Proceedings of the 13th International Heat Transfer Conference, THE-24.

Schultz, D.L., Jones, T.V., 1973. Heat transfer measurements in short-duration hypersonic facilities, AGARD-AG-165.

Shah, R.K., London, A.L., 1978. Laminar flow forced convection in ductsSupplement 1 to Advances in Heat Transfer. Academic, NY.

Wang, Z., Yeo, K.S., Khoo B.C., 2003. Numerical simulation of laminar channel flow over dimpled surface. AIAA 2003-3964.